Response characteristics of optical sensors for oxygen: models based on a distribution in τ_o *or* k_q

The Analyst

Andrew Mills†

Department of Chemistry, University of Wales Swansea, Singleton Park Swansea, UK SA2 8PP

Received 18th March 1999, Accepted 12th July 1999

The features of two popular models used to describe the observed response characteristics of typical oxygen optical sensors based on luminescence quenching are examined critically. The models are the 'two-site' and 'Gaussian distribution in natural lifetime, τ_o,' models. These models are used to characterise the response features of typical optical oxygen sensors; features which include: downward curving Stern–Volmer plots and increasingly non-first order luminescence decay kinetics with increasing partial pressures of oxygen, pO_2. Neither model appears able to unite these latter features, let alone the observed disparate array of response features exhibited by the myriad optical oxygen sensors reported in the literature, and still maintain any level of physical plausibility. A model based on a Gaussian distribution in quenching rate constant, k_q, is developed and, although flawed by a limited breadth in distribution, ρ, does produce Stern-Volmer plots which would cover the range in curvature seen with real optical oxygen sensors. A new 'log-Gaussian distribution in τ_o or k_q' model is introduced which has the advantage over a Gaussian distribution model of placing no limitation on the value of ρ. Work on a 'log-Gaussian distribution in τ_o' model reveals that the Stern-Volmer quenching plots would show little degree in curvature, even at large ρ values and the luminescence decays would become increasingly first order with increasing pO_2. In fact, with real optical oxygen sensors, the opposite is observed and thus the model appears of little value. In contrast, a 'log-Gaussian distribution in k_o' model does produce the trends observed with real optical oxygen sensors; although it is technically restricted in use to those in which the kinetics of luminescence decay are good first order in the absence of oxygen. The latter model gives a good fit to the major response features of sensors which show the latter feature, most notably the $[Ru(dpp)_3^{2+}(Ph_4B^-)_2]$ in cellulose optical oxygen sensors. The scope of a log-Gaussian model for further expansion and, therefore, application to optical oxygen sensors, by combining both a log-Gaussian distribution in k_o with one in τ_o is briefly discussed.

Introduction

The detection and monitoring of oxygen is important in many areas,[1,2] including: environmental studies (ambient levels in the atmosphere or dissolved in river, lake or sea waters), patient monitoring (blood gas or breath analysis) and many industrial processes (as diverse as fermentation or sewage treatment). As a consequence, sensing for oxygen is a very important area in analytical chemistry; an area dominated for nearly 4 decades by electrochemical devices, most notably the Clark cell, an oxygen membrane polarographic device.[2]

In the last decade, the optical oxygen sensor has emerged as a real competitor to the Clark cell, replacing, as it does, costly wires with cheap fibre optics, eliminating electrical interference effects and removing the need for expensive and time-consuming sensor preparation.[1,3] Optical sensors for oxygen are cheap enough to be made disposable; they are also robust and capable of very remote, but rapid sensing. The potential of optical oxygen sensors has prompted many research groups to work on their development in recent years. And yet, despite the intensity of this research, there remain key features of the response characteristics of optical oxygen sensors that have eluded a unifying physical model.[4] Such a model, if it is to be had, would provide a better understanding of the underlying processes involved and enable the generation of accurate calibration curves from only a few experimental points. A unifying model would also lead to improvements in sensor development, moving from its current, strongly empirical-based approach to, eventually, a designer-based status, in which optical oxygen sensors are designed and made with specific response features, in keeping with their different areas of application.

The majority of optical oxygen sensors work on the principle of the quenching of the luminescence of a dye by oxygen; the higher the level of oxygen the lower the level of luminescence.[1,3] The lumophores that have been used for this purpose are many and varied and include ruthenium(II) diimine complexes, most notably tris(4,7-diphenyl-1,10-phenanthroline) ruthenium(II), $[Ru(dpp)_3^{2+}]$, and Pt(II) and Pd(II) porphyrins.[1] In its simplest form, an optical oxygen sensor can be generated using a solution of any suitable lumophore (*i.e.*, one that is quenched by oxygen). Under such conditions, the lumophore is usually dispersed homogeneously throughout the solution and the quenching of its luminescence fits a simple Stern–Volmer equation,[1] *i.e.*

$$\tau_o/\tau = I_o/I = 1 + K_{SV}.pO_2 \quad (1)$$

where K_{sv} is the Stern–Volmer constant and (τ and τ_o) and (I and I_o) are the lifetimes and intensities of luminescence in the presence and absence of oxygen, respectively; the latter at a partial pressure of pO_2. The Stern–Volmer constant is, of course, a composite parameter equal to the product of the quenching rate constant, k_q, and the natural lifetime of the lumophore, τ_o, *i.e.*, $K_{SV} = k_q.\tau_o$.

The above crude example of an oxygen optical sensor, although simple to make and with easily modeled response features, is not really a practical device. Instead, with most optical oxygen sensors that can be construed as practical, the

† Present address: Department of Pure and Applied Chemistry, University of Strathclyde, Thomas Graham Building, 295 Cathedral Street, Glasgow, UK G1 1XL. E-mail: A.Mills@strath.ac.uk

lumophore is dispersed on and/or in a solid substrate, such as a sol–gel,[5] metal oxide[6] or, most often, a polymer.[1,7] In such systems, the Stern–Volmer intensity plot, *i.e.*, I_o/I *versus* pO_2, often exhibits a reproducible and characteristic negative deviation from linearity; the degree of curvature varying from sensor to sensor with no apparent logical cause. In the latter cases, the lumophore is usually the same and it is simply the encapsulating medium that is altered. Fig. 1[8–11] illustrates a selection of such Stern–Volmer intensity plots. With the many sensors that exhibit such curvature, lifetime studies also show that the kinetics of the luminescence decays in the presence, and often in the absence, of oxygen are usually no longer simple first order and so cannot be adequately described by the single parameters, τ or τ_o, respectively.

Several models[12–22] have been proposed to describe and explain the downwardly curved Stern–Volmer intensity plots associated with most optical oxygen sensors. Most of these models attribute the latter feature to the micro-heterogeneous nature of the lumophore/encapsulating medium type sensor; a feature that manifests as a distribution of spectroscopically different sites. In this paper the problems, as well as positive features, of the two major models used for interpreting and predicting trends in the response characteristics of optical oxygen sensors, namely, the 'two-site'[12–14] and the 'Gaussian distribution in τ'[17–19] models, are identified. From the understanding gained, a third model, the 'log-Gaussian' model is introduced. In the first of two papers, the effect of the predicted response characteristics of an optical oxygen sensor in which there is a log-Gaussian distribution in τ_o or k_q is examined. The predictions are tested using the results from real optical sensors for oxygen and the results discussed.

Experimental

Most of the experimental data used to test the various models discussed in this paper were taken from the referenced literature. The exception is the results for the tetraphenyl borate salt of tris(4,7-diphenyl-1,10-phenanthroline) ruthenium(II), *i.e.*, $[Ru(dpp)_3^{2+}(Ph_4B^-)_2]$, encapsulated in the polymer, cellulose acetate. The method of preparation of $[Ru(dpp)_3^{2+}(Ph_4B^-)_2]$ is described elsewhere.[23] The typical solution used for casting films comprised a mixture of (a) a solution containing 2 mg of $[Ru(dpp)_3^{2+}(Ph_4B^-)_2]$ dissolved in 1 mL acetone and (b) 10 g of a 20% m/v solution of cellulose acetate in acetone. The final film solution was cast onto cut microscope glass slides (dimensions: 4 × 0.9 × 0.1 cm) through a 100 μm thick brass template with a rectangular hole (0.5 × 1 cm) and then allowed to dry in a desiccator for at least 3 h. The typical film thickness was 25 μm. Luminescence decay measurements were performed using a Nd/YAG Spectron (Rugby, UK) nano-second laser with an Applied Photophysics (London, UK) laser kinetic spectrophotometer monitoring system. The average trace from 32 shots of laser excitation was collected on a Gould Instruments (Ilford, UK) OS4072 digital storage oscilloscope and transferred to a microcomputer for kinetic analysis. Unless stated otherwise, all illustrated Stern–Volmer plots are based on intensity, rather than lifetime, measurements.

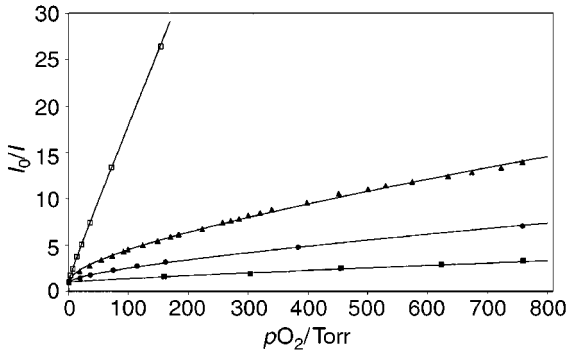

Fig. 1 Stern–Volmer plots of I_o/I *versus* pO_2 for the following optical oxygen sensors: [Pd(II)OEPK] in PVC[8] (□), $[Pt(dpp)(CN^-)_2]$ in silicone rubber[9] (▲), $[Ru(dpp)_3^{2+}(DS^-)_2]$ in silicone rubber[10] (●) and $[Ru(dpp)_3^{2+}(Ph_4B^-)_2]$ in cellulose acetate (■), this work. The solid lines have been calculated using eqn. (19) and the optimised values of ρ and K_{mdl} are given in Table 1.

The two-site model[12–14]

In all the models which are described in this paper, the general assumption is made that there is a distribution of quenching sites within the encapsulating medium and that at any one type of site, *i*, the lumophore molecules are quenched by oxygen so that their lifetime, τ_i, is given by the expression:

$$\tau_i = \tau_{o,i}/(1 + \tau_{o,i}.k_{q,i}pO_{2,i}) \quad (2)$$

where, $\tau_{o,i}$ is the lifetime of the lumophore in the absence of oxygen and $k_{q,i}$ is the rate constant for quenching the lumophore by oxygen at a local partial pressure of $pO_{2,i}$. As the name suggests, in the two site model it is assumed that there are only two types of quenching sites present in the encapsulation medium, each resulting in a characteristic natural lifetime and quenching rate constant for the lumophore molecules at those sites, *i.e.*, $\tau_{o,1}$ and k_1 and $\tau_{o,2}$ and k_2, respectively. In this model it is also assumed that there is no difference in the partial pressures of oxygen at the two sites and that $pO_{2,i}$ is proportional to the ambient partial pressure of oxygen, pO_2, if not equal to it. Unless stated otherwise it is assumed throughout this paper that $pO_{2i} = pO_2$. Under such conditions, it can be shown that the modified Stern–Volmer equation has the following form:

$$\frac{I_o}{I} = \frac{1}{f_1(1+k_1\tau_{o,1}pO_2)+(1-f_1)/(1+k_2\tau_{o,2}pO_2)} \quad (3)$$

Where, f_1 is the fraction of the overall total number of sites that have a natural lifetime $\tau_{o,1}$ and a quenching rate constant k_1. The above equation has been used extensively to describe the downward curving Stern–Volmer plots associated with most optical oxygen sensors. Table 1 provides the values of K_{SV1} (= $k_1\tau_{o,1}$) and K_{SV2} (= $k_2.\tau_{o,2}$) which give a good fit to the Stern-Volmer plots illustrated in Fig. 1.

The problem with the two site model is the lack of consistency between the values of f_1, K_{SV1} and K_{SV2}, obtained from the Stern-Volmer plot of the intensity data, and the

Table 1 Characteristics of some typical optical oxygen sensors

Lumophore[a]	Encapsulation medium	f_1	K_{SV1}/Torr^{-1}	K_{SV2}/Torr^{-1}	K_{mdl}/Torr^{-1}	ρ	Ref.
[Pd(II)OEPK]	Polystyrene	0.152	2.7	0.142	0.22	1.12	8
$[Pt(dpp)(CN^-)_2]$	Silicone rubber (RTV 732; GE)	0.893	0.0588	0.00135	0.086	3.15	9
$[Ru(dpp)_3^{2+}(DS^-)_2]$	Silicone rubber (E4; Wacker)	0.74	0.0346	0.00161	0.0188	2.5	10
$[Ru(dpp)_3^{2+}(BPh_4^-)_2]$	Cellulose acetate	0.498	0.00134	0.00809	0.0033	1.4	11, this work

[a] OEPK: octaethylporphyrin ketone; DS^-: dodecyl sulfate; ph: 1,10-phenanthroline.

luminescence decay results obtained with the same optical oxygen sensor. The luminescence decay of a *multi-exponential* system, *i.e.*, the $I(t)$ *versus* t profile, is described by:

$$I(t) = \sum \alpha_i \exp(-t/\tau_i) \quad (4)$$

where α_i is the pre-exponential factor associated with the luminescence decay of sites i. Demas and his coworkers[17] have introduced the feature of a pre-exponential weighted mean lifetime, τ_M, defined as follows:

$$\tau_M = \sum \alpha_i \tau_i / \sum \alpha_i \quad (5)$$

It follows that $\tau_{o,M} = \sum \alpha_i \tau_{o,i} / \sum \alpha_i$. These workers proved[17] that in the absence of static quenching:

$$I_o/I = \tau_{o,M}/M \quad (6)$$

In all reported examples of optical oxygen sensors eqn. (6) appears to hold, *i.e.*, there appears to be no evidence of static quenching with any optical oxygen sensor.

In the two-site model, eqn. (5) reduces to:

$$\tau_M = \alpha_1 \tau_1 + (1 - \alpha_1)\tau_1 \quad (7)$$

assuming, for simplicity, $\sum \alpha_i = 1$. If the two-site model provides a true description of the response features of an oxygen sensor, then *the value of* f_1 (*from the Stern–Volmer plot* I_o/I *(or* $\tau_{o,M}/\tau_M$*)* versus pO_2*) should be equal to that of* α_1 *at all values of* pO_2. This prediction is usually *not* fulfilled with most optical oxygen sensors that have been fitted to a two site model. For example, Demas *et al.*[12]. noted, for the $[Ru(bpy)_3^{2+}(ClO_4^-)_2]$ in RTV-118 silicone rubber oxygen sensor, that α_1 varies from 0.16–0.31 over the pO_2 range 0–760 Torr (1 Torr = 133.322 Pa), whereas from the Stern–Volmer plot the value of f_1 appears to be 0.4. Apparent dramatic changes in α_1 with increasing pO_2 have also been noted for different optical oxygen sensors by others.[10,11,20]

Although the luminescence decay curves exhibited by many optical oxygen sensors can be fitted to two exponentials, some appear to require three,[12] introducing the idea of a three site model. However, as with the two-site model, with such systems the variations in τ_i and α_i with increasing pO_2 are inconsistent with any physically plausible cause. Thus, the two- and three-site models are used nowdays simply as useful good quality fitting routines.

Table 2[24–26] lists the typical, apparently very disparate response features, which have been observed with optical oxygen sensors. It can be seen that in the absence of oxygen some optical oxygen sensors exhibit first order decay kinetics, but that these change to multi-exponential with the introduction of oxygen. With other sensors the kinetics of luminescence decay, with or without oxygen present, require two or three exponentials in order to be described adequately. In general, the more exponentials needed to describe the decay kinetics, the more curved the Stern–Volmer plot. In order to be useful, any model should ideally be able to embrace all these features and still have a reasonable physical basis.

A Gaussian distribution model

Although the two- and three-site models of the response features of optical oxygen sensors have been rejected as models with any physical meaning, it is a mistake to abandon the principle of a multi-site model completely. It seems logical to wonder what the response features of an optical oxygen sensor would be if it comprised a much bigger distribution in quenching sites; a distribution which can be described by a simple statistical function? Demas and his co-workers[17–19] were the first to address this question with their work on a model based on a 'Gaussian distribution in $\tau_{o,i}$'; $k_{q,i}$ and $pO_{2,i}$ remaining constant and equal to k_q and pO_2, respectively.

For a Gaussian distribution, the number of sites i, *i.e.*, n_i, is related to the modal number of sites, n_{mdl}, (*i.e.*, the most frequently occurring type of site in the distribution) by the expression:

$$n_i/n_{mdl} = \exp(-x^2) \quad (8)$$

where x is related to the value of $\tau_{o,i}$ associated with sites i and that associated with the modal number of sites, *i.e.*, $\tau_{o,mdl}$, through the expression:

$$x = \{(\tau_{o,i}/\tau_{o,mdl}) - 1\}/\rho \quad (9)$$

where ρ is a measure of the spread of the distribution in the natural radiative lifetime of the lumophore, $\tau_{o,i}$. Although Demas and his co-workers[17–19] focussed on a model based on a Gaussian distribution in $\tau_{o,i}$, it follows that in a model in which there is, instead, a Gaussian distribution in $k_{q,i}$; with $\tau_{o,i}$ and $pO_{2,i}$ invariant for all sites and equal to τ_o and pO_2, respectively, that:

$$x = \{(k_{q,i}/k_{q,mdl}) - 1\}/\rho \quad (10)$$

Note that the effect of a Gaussian distribution in $pO_{2,i}$, with $\tau_{o,i}$ and $k_{q,i}$ constant for all sites, is indistinguishable from, and will produce the same trends as, a Gaussian distribution in $k_{q,i}$; with $\tau_{o,i}$ and $pO_{2,i}$ invariant for all sites; thus, to avoid repetition, only the latter case will be considered throughout this work.

For a Gaussian distribution in $\tau_{o,i}$ the variation in the fraction of sites i compared with the modal number of sites, *i.e.*, n_i/n_{mdl}, as a function of the ratio $\tau_{o,i}/\tau_{o,mdl}$ can be calculated using eqns. (8) and (9), given a value for the breadth of the distribution, ρ. A similar exercise can be performed for a Gaussian distribution in $k_{q,i}$ using eqns. (8) and (10). The two profiles are the same for any given value of ρ, as illustrated by the results in Fig. 2 which show the calculated variation in n_i/n_{mdl} as a function of the ratio $\tau_{o,i}/\tau_{o,mdl}$ (or $k_{q,i}/k_{q,mdl}$) for values of ρ spanning the range 0.1–2. The important feature to note from this work is that it has to be assumed that $\tau_{o,i}$ (or, $k_{q,i}$) cannot be < 0, *i.e.*, x cannot be $< -1/\rho$. Thus, as the value of ρ is increased, the original Gaussian distribution becomes increasingly distorted, see Fig. 2, and the model accordingly becomes more detached from any likely physical reality. This latter feature led Demas and his co-

Table 2 Response features of typical oxygen optical sensors

Stern–Volmer plot	Lifetime studies: No. of exponentials		Examples		Ref.
	N_2	O_2	Lumophore	Encapsulating medium	24
Linear	1	2	PtOEPK	PVC	24
Linear	2	2	PtOEPK	PS	24
Slightly curved	1	2	PdOEPK	PVC	24
			$[Ru(dpp)_3^{2+}(ClO_4^-)_2]$	Poly(dimethyl siloxane) diacetoxy polymer	25
			$[Ru(dpp)_3^{2+}(Ph_4B^-)_2]$	Cellulose acetate	11, 23, this work
Curved	2	2	$[Ru(bpy)_3^{2+}(ClO_4^-)_2]$	RTV-118 silicone rubber	12
			$[Ru(dpp)_3^{2+}(ClO_4^-)_2]$	Polystyrene	26
			$[Ru(dpp)_3^{2+}(ClO_4^-)_2]$	PVC	20
Very curved	3	3	$[Ru(phen)_3^{2+}(ClO_4^-)_2]$	RTV-118 silicone rubber	12
			$[Ru(dpp)_3^{2+}(ClO_4^-)_2]$	Ethyl cellulose or polystyrene	20

workers[18,19] to limit their modeling to ρ values ≤ 0.35 and is a clear drawback to using a Gaussian distribution in $\tau_{o,i}$ or, $k_{q,i}$.

For a Gaussian distribution in $\tau_{o,i}$ it can be shown, using eqns. (2), (6), (8) and (9), that the ratio of the total unquenched to total quenched luminescence intensity, *i.e.*, I_o(total)/I(total), is related to pO_2 through the expression:

$$\frac{I_o(\text{total})}{I(\text{total})} = \frac{\int_{-1/\rho}^{\infty} \tau_{o,mdl}(1+\rho x)\exp(-x^2)dx}{\int_{-1/\rho}^{\infty} \{\tau_{o,mdl}(1+\rho x)\exp(-x^2)/[1+k_q\tau_{o,mdl}pO_2(1+\rho x)]\}dx} \quad (11)$$

For a Gaussian distribution in $k_{q,i}$ it can be shown that the ratio of the total unquenched to total quenched luminescence intensity, *i.e.*, I_o(total)/I(total), is related to pO_2 through the expression:

$$\frac{I_o(\text{total})}{I(\text{total})} = \frac{\int_{-1/\rho}^{\infty} \exp(-x^2)dx}{\int_{-1/\rho}^{\infty} \{\exp(-x^2)/[1+k_{q,mdl}\tau_o pO_2(1+\rho x)]\}dx} \quad (12)$$

It is useful at this stage to define, for a Gaussian distribution in τ_i, a unitless parameter, θ, which is related directly to the partial pressure of oxygen, pO_2, *i.e.*,

$$\theta = k_q\tau_{o,mdl}pO_2 \quad (13)$$

Eqn. (13) allows a series of Stern–Volmer plots (I_o(total)/I(total) *versus* θ) to be calculated using eqn. (11) and different values of ρ. In making these calculations, it was assumed initially that 80 different sites existed spanning the range $x = -4$ to $x = 4$, in steps of $\Delta x = 0.1$. The number of sites was reduced usually with the additional necessary condition that only sites with $x \geq -1/\rho$ can exist, *i.e.*, $\tau_{o,i}$ (or, $k_{q,i}$) cannot be < 0. Additional work showed that increasing the range in x and/or decreasing the step size in × increased the computational time with little effect on the overall results. The results of these calculations are illustrated in Fig. 3(a) and are very similar to those reported by Demas *et al*.[18] for the same model. Most notable amongst these results is that apparent high degree of linearity in the Stern–Volmer plots even when the breadth of the distribution is so large as to make the model unrealistic, *i.e.* > 0.35. This finding further undermines the usefulness of the model, since from Fig. 1 and Table 2 it is clear that many optical oxygen sensors produce Stern–Volmer plots with pronounced curvature. Demas and his co-workers[17–19] were able to get round the lack of curvature exhibited by their initial Gaussian model by suggesting that there may be more than one Gaussian distribution, both narrow, but each with a different k_q value. Under these conditions most of the curved Stern–Volmer plots associated with optical oxygen sensors can be generated, although, as with the two-site model to which it is closely related, it does not appear that the bimodal Gaussian model has any physical significance.

It is useful also to examine what effect a Gaussian distribution in k_i will have on an optical oxygen sensor. This can be done using the same approach as above, but this time using eqn. (12) and defining $\theta = k_{q,mdl}\tau_o pO_2$. The results of this work are illustrated in Fig. 3(b) and are strikingly dissimilar to those in Fig. 3(a) in that the degree of curvature exhibited by the plots in the former figure increases markedly with increasing value of ρ. In the Stern-Volmer plots illustrated in Fig. 3(b) the range of curvature is well within that observed for most optical oxygen sensors. And yet this curvature may simply arise from the distortion of the Gaussian distribution with increasing value of ρ; a distortion that makes its suitability, as a physical model of optical oxygen sensors, unlikely. However, the results are encouraging enough to merit the investigation of other possible statistical distributions and this has led to the following work with log-Gaussian distributions.

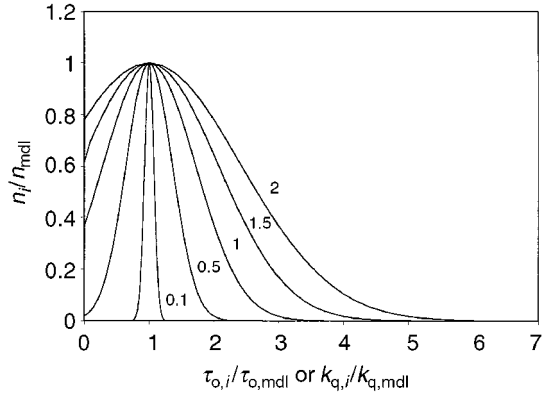

Fig. 2 Plot of the calculated ratio of fraction of sites i compared to the modal number of sites, *i.e.*, n_i/n_{mdl}, {$= \exp(-x^2)$} as a function of the ratio $\tau_{o,i}/\tau_{o,mdl}$ or $k_{q,i}/k_{q,mdl}$, calculated using a Gaussian distribution model, *i.e.* eqns. (8) and (9), or (8) and (10), respectively. Each profile corresponds to a different value of ρ, *i.e.*, from inside-out ρ = 0.1, 0.5, 1, 1.5, 2, respectively.

A log-Gaussian distribution model

The log-Gaussian distribution is no stranger to heterogeneous systems. It has been used to fit successfully kinetic data from semiconductor surface states, colloidal semiconductors and fluorescent probes attached to biological membranes.[27,28] A log-Gaussian distribution in the rate constant for a process is usually taken as a reflection of a Gaussian distribution in activation free energies for that process.

If there is a log-Gaussian distribution in $\tau_{o,i}$, *i.e.*:

$$\rho x = \ln(\tau_{o,i}/\tau_{o,mdl}) \quad (14)$$

Alternatively, if there is a log-Gaussian distribution in $k_{o,i}$, *i.e.*:

$$\rho x = \ln(k_{o,i}/k_{o,mdl}) \quad (15)$$

For a log-Gaussian distribution in $\tau_{o,i}$, the fraction of sites i compared with the modal number of sites, *i.e.*, n_i/n_{mdl}, as a

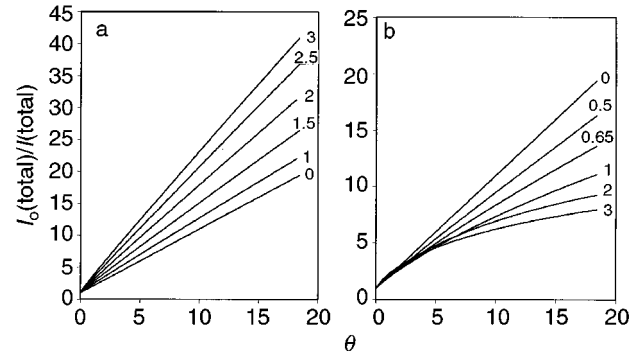

Fig. 3 Model generated Stern–Volmer quenching plots of I_o(total)/I(total) *versus* θ, calculated for a Gaussian distribution in: (a) natural lifetime of the lumophore, *i.e.*, $\tau_{o,i}$, using eqns. (11) and (13) with ρ = (from bottom to top): 0, 1, 1.5, 2, 2.5 and 3, respectively; or (b) oxygen quenching rate constant, $k_{q,i}$, using eqn. (12) and $\theta = k_{q,mdl}.\tau_o.pO_2$, with ρ = (from top to bottom): 0, 0.5, 0.65, 1, 2, and 3, respectively.

function of the ratio $\tau_{o,i}/\tau_{o,mdl}$ can be calculated using eqns. (8) and (14), for any value of ρ. A similar exercise can be performed for a Gaussian distribution in $k_{q,i}$ using eqns. (8) and (15) Fig. 4 illustrates the results of this work, *i.e.*, a plot of n_i/n_{mdl} *versus* $\tau_{o,i}/\tau_{o,mdl}$ (or $k_{q,i}/k_{q,mdl}$) for a range of ρ values from 0.1 to 2. From these results it can be seen that, unlike a Gaussian distribution, a log-Gaussian distribution has the attractive feature of generating $\tau_{o,i}/\tau_{o,mdl}$ (or $k_{o,I}/k_{o,mdl}$) values that are ≥ 0, whatever the value of ρ or x, *cf.* Fig. 4 and Fig. 2.

From the equations for a log-Gaussian distribution in $\tau_{o,i}$ it follows that the ratio of the total unquenched to total quenched luminescence intensity, *i.e.*, I_o(total)/I(total), is related to θ [related directly to pO_2, *cf.* eqn. (13)] through the expression:

$$\frac{I_o(\text{total})}{I(\text{total})} = \frac{\int_{-\infty}^{\infty} \exp(\rho x)\exp(-x^2)\mathrm{d}x}{\int_{-\infty}^{\infty} \{\exp(\rho x)\exp(-x^2)/[1+\theta\exp(\rho x)]\}\mathrm{d}x} \quad (16)$$

Using eqn. (16) and different values of ρ, a series of Stern–Volmer plots (I_o(total)/I(total) *versus* θ) were generated and the results of this work are illustrated in Fig. 5(a). As with a Gaussian distribution in $\tau_{o,i}$ it appears that only when the distribution in site natural lifetimes is large, *i.e.*, $\rho > 1$, does the Stern–Volmer plot begin to show some signs of curvature.

For a log-Gaussian distribution in $\tau_{o,i}$ at any time t after an initial pulse of excitation light, the number of sites i present is given by the expression:

$$n_{i,t} = n_i\exp-[(1/\tau_{o,i} + k_q pO_2)t] \quad (17)$$

If we define a normalised time unit, τ^*, as $\tau^* = t/\tau_{o,mdl}$, then it is also possible to predict what the luminescence decay profiles will look like with increasing θ (*i.e.*, increasing pO_2) using the following expression:

$$\frac{I_{\tau^*}}{I_{\tau^*=0}} = \frac{\int_{-\infty}^{\infty} \exp(-x^2)\exp-[1+\theta\exp(\rho x))\tau^*\exp(-\rho x)]\mathrm{d}x}{\int_{-\infty}^{\infty} \exp(-x^2)\mathrm{d}x} \quad (18)$$

Fig. 6 illustrates the results of a series of calculations using eqn. (18), of the $I_{\tau^*}/I_{\tau^*=o}$ *versus* τ^* profiles for a log-Gaussian distribution in $\tau_{o,i}$ with increasing θ, with ρ set at 1. The insert diagram illustrates the first-order plot of the data and shows that as θ, *i.e.*, the partial pressure of oxygen, is increased, the decay kinetics become increasingly better first-order. This effect is typical of a model in which there is a distribution in $\tau_{o,i}$, but not in $k_{q,i}$, which is set at a constant value k_q. However, it is also a feature that is not usually seen with real optical oxygen sensors. As noted previously, *cf.* Table 2, with real optical sensors the decay kinetics, if anything, become less first order with increasing pO_2. The lack of a marked degree of curvature in the model-generated Stern–Volmer plots with increasing ρ value and the predicted increase in the first order nature of the luminescence decay kinetics with increasing pO_2 makes it unlikely that a log-Gaussian distribution in $\tau_{o,i}$ is a useful model for the response features of any optical oxygen sensors reported to date.

From the equations for a log-Gaussian distribution in $k_{q,i}$ it follows that the ratio of the total unquenched to total quenched luminescence intensity, *i.e.*, I_o(total)/I(total), is related to θ ($= k_{q,mdl}.\tau_o.pO_2 = K_{mdl}.pO_2$)) through the expression:

$$\frac{I(\text{total})}{I(\text{total})} = \frac{\int_{-\infty}^{\infty} \exp(-x^2)\mathrm{d}x}{\int_{-\infty}^{\infty} \{\exp(-x^2)/[1+\theta\exp(\rho x)]\}\mathrm{d}x} \quad (19)$$

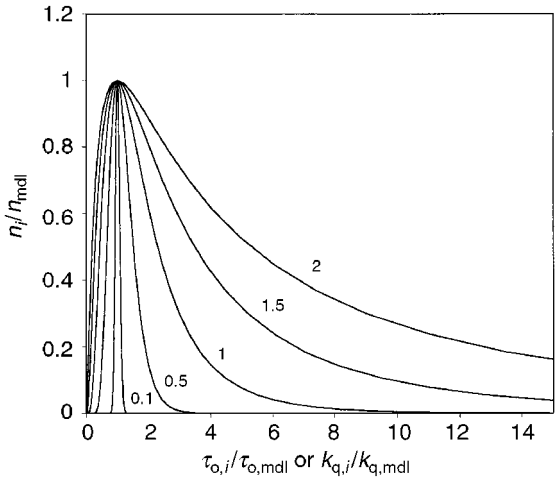

Fig. 4 Plot of the calculated ratio of fraction of sites i compared to the modal number of sites, *i.e.*, n_i/n_{mdl}, { = $\exp(-x^2)$} as a function of the ratio $\tau_{o,i}/\tau_{o,mdl}$ or $k_{q,i}/k_{q,mdl}$, calculated using a log-Gaussian distribution model, *i.e.*, eqns (8) and (14), or (8) and (15), respectively. Each profile corresponds to a different value of ρ, *i.e.*, from inside-out ρ = 0.1, 0.5, 1, 1.5, 2, respectively.

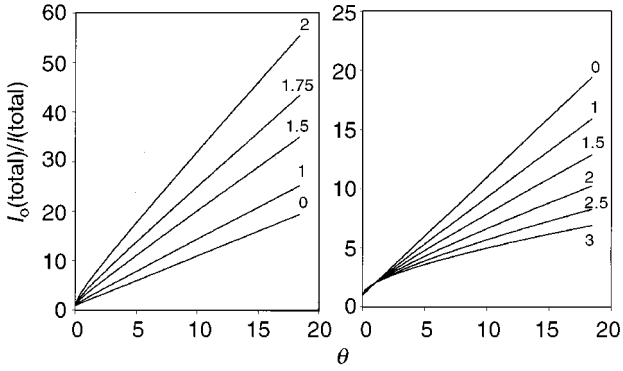

Fig. 5 Model generated Stern–Volmer quenching plots of I_o(total)/I(total) *versus* θ, calculated for a log-Gaussian distribution in: (a) natural lifetime of the lumophore, *i.e.*, $\tau_{o,i}$, using eqns. (16) and (13) with ρ = (from bottom to top): 0, 1, 1.5, 1.75, and 2, respectively; or (b) oxygen quenching rate constant, $k_{q,i}$, using eqn. (19) and $\theta = k_{q,mdl}.\tau_o pO_2$, with ρ = (from top to bottom): 0, 1, 1.5, 2, 2.5 and 3, respectively.

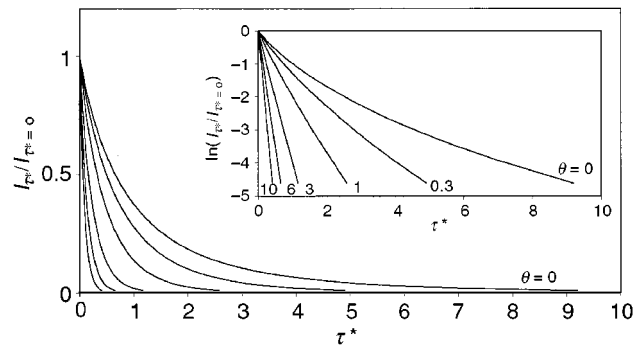

Fig. 6 Model-generated transient luminescence decay profiles for an optical oxygen sensor which exhibits a log-Gaussian distribution in $\tau_{o,i}$. The profiles were calculated using eqn. (18), for a sensor with ρ = 1 and θ (from right to left) = 0, 0.3, 1, 3, 6 and 10. The insert diagram illustrates the first-order plots of the kinetic data shown in the main diagram.

Using eqn. (19) and different values of ρ, a series of Stern–Volmer plots (I_o(total)/I(total) *versus* θ) were generated and the results of this work are illustrated in Fig. 5(b). In contrast to the profiles generated based on a log-Gaussian distribution in $\tau_{o,i}$, *cf.* Fig. 5(a), a log-Gaussian distribution in $k_{q,i}$ generates Stern-Volmer profiles of increasing curvature with increasing ρ. Indeed, in a previous paper[4] eqn. (19) was used to fit a number of Stern–Volmer plots, of widely differing curvature, reported for real optical oxygen sensors. The model requires only two parameters (ρ and K_{mdl}) to provide a good fit, rather than the usual three or more associated with most other models.

However, the model does not embrace all the kinetic features of those real optical sensors; features which are summarised in Table 2. Most notably, a log-Gaussian distribution in $k_{q,i}$ model assumes that there is no distribution in $\tau_{o,i}$ so that at $\theta = 0$, *i.e.*, $pO_2 = 0$, the overall luminescence decay should fit perfectly first-order kinetics. In practice, only a few optical oxygen sensors show this feature. Fig. 1 illustrates Stern–Volmer data for some of the reported optical oxygen sensors which appear to show good first-order decay kinetics in the absence of oxygen, and increasingly worse first order kinetics with increasing pO_2; the results are summarised in Table 1. The solid lines in Fig. 1 are the lines of best fit calculated using eqn. (19) and the optimised values for ρ and K_{mdl} given in Table 1. Simple methods for finding the values of ρ and K_{mdl} that give the best fit of the model-generated curves to the real Stern–Volmer data are given elsewhere.[4].

If the log-Gaussian distribution in $k_{q,i}$ model is really appropriate to such systems, although they be limited in number, it must also be able to predict accurately the decay kinetics exhibited by such systems. Unfortunately, very few details have been reported on the decay kinetics of the optical oxygen sensors listed in Table 1 and illustrated in Fig. 1. Thus, in order to test the model, a kinetic study was carried out on one of the optical oxygen sensors which gives a curved Stern–Volmer plot and exhibits good first-order luminescence decay kinetics at $pO_2 = 0$, but not at $pO_2 \gg 0$; the optical oxygen sensor was $[Ru(dpp)_3^{2+}(Ph_4B^-)_2]$ in non-plasticised cellulose acetate.[11,23] The results of the kinetic study and the Stern–Volmer plot of the lifetime data are illustrated by the data points in Fig. 7 and its insert diagram, respectively.

For a log-Gaussian distribution in $k_{q,i}$ at any time t after an initial pulse of light the number of sites i present is given by the expression:

$$n_{i,t} = n_i \exp[-(1/\tau_o + k_{q,i}pO_2)t] \quad (20)$$

It follows that $I_{\tau^*}/I_{\tau^*=0}$ *versus* τ^* profiles can be generated for any value of θ using the expression:

$$\frac{I_{\tau^*}}{I_{\tau^*=0}} = \frac{\int_{-\infty}^{\infty} \exp(-x^2)\exp-[1+\theta\exp(\rho x))\tau^*]dx}{\int_{-\infty}^{\infty} \exp(-x^2)dx} \quad (21)$$

In order to convert the model generated $I_{\tau^*}/I_{\tau^*=0}$ *versus* τ^* plot for any value of θ and ρ, into one which can be compared with the data for a real optical sensor, optimised values for τ_o and K_{mdl} are needed. The former converts the unitless time parameter, τ^* to real time, t, ($\tau^* = t/\tau_o$) and the latter converts the unitless oxygen concentration parameter, θ, to real pO_2 ($\theta = K_{mdl}pO_2$). For the simple optical system under test, a value for τ_o can be gleaned from a first-order plot of the luminescence *versus* time profile recorded in the absence of oxygen; the resulting gradient of the straight line $= -1/\tau_o$. Using this approach τ_o was found to be 5.85 μs for the $[Ru(dpp)_3^{2+}(Ph_4B^-)_2]$ in cellulose acetate optical sensor. Optimised values for K_{mdl} and ρ can be obtained from the Stern–Volmer plot of the real data, either in the form of I_o/I or $\tau_{o,M}/\tau_M$ *versus* pO_2. The latter requires finding the values of K_{mdl} and ρ which, when used with eqn. (19) of the model, generates a curve of best fit to the real Stern–Volmer data associated with the optical oxygen sensor under test. From Table 2 it can be seen that the optimised values for K_{mdl} and ρ for the $[Ru(dpp)_3^{2+}(Ph_4B^-)_2]$ in cellulose acetate oxygen sensor were found to be 0.0033 $Torr^{-1}$ and 1.4, respectively. Using these values, the log-Gaussian distribution in $k_{q,i}$ model eqn. (19) and $\theta = K_{mdl}pO_2$ were used to generate the solid line in the insert diagram in Fig. 7 which provides a good fit to the observed Stern–Volmer plot of the lifetime data for the $[Ru(dpp)_3^{2+}(Ph_4B^-)_2]$ in cellulose acetate optical oxygen sensor.

The optimised parameters for τ_o (5.85 μs), K_{mdl} (0.0033 $Torr^{-1}$) and ρ (1.4) were used in eqn. (21) to generate the solid lines luminescent decay profiles for the $[Ru(dpp)_3^{2+}(Ph_4B^-)_2]$ in cellulose acetate oxygen sensor illustrated in the main diagram of Fig. 7 and recorded for a range of different pO_2 levels; the fits appear reasonable and encouraging.

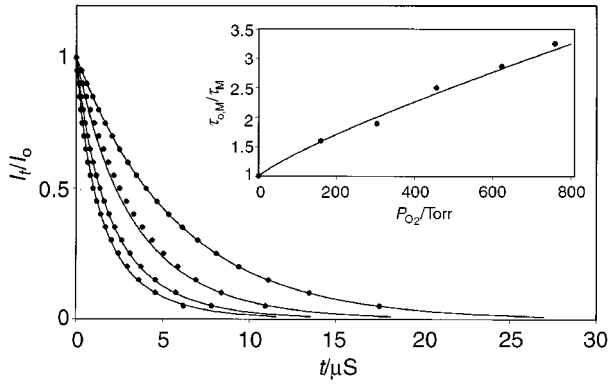

Fig. 7 Transient decay profiles (●) recorded for a $[Ru(dpp)_3^{2+}(Ph_4B^-)_2]$ in cellulose acetate oxygen optical sensor when exposed to the following (top to bottom) partial pressures of oxygen: 0, 160, 456 and 760 Torr, respectively. The solid lines are 'log-Gaussian distribution in $k_{q,i}$' model generated decay profiles, calculated using eqn. (21) and τ_o = 5.85 μs, K_{mdl} = 0.0033 $Torr^{-1}$ and ρ = 1.4. The insert diagram illustrates the Stern–Volmer plot based on lifetime measurements (●), *i.e.*, $\tau_{o,M}/\tau_M$ *versus* pO_2, for the $[Ru(dpp)_3^{2+}(Ph_4B^-)_2]$ in cellulose acetate oxygen optical sensor. In this insert diagram the solid line is the 'log-Gaussian distribution in $k_{q,i}$' model generated curve, calculated using eqn. (19) with K_{mdl} = 0.0033 and ρ = 1.4.

Conclusion

The 'two-site' and 'Gaussian distribution in natural lifetime, τ_o,' models, used to describe the observed response characteristics of typical oxygen optical sensors based on luminescence, although good fitting procedures (especially the former), do not generate fitting parameters which have any likely physical reality. Ideally, a model should be able to unite all the response features of typical optical oxygen sensors, including downward curving Stern–Volmer plots and increasingly non-first order luminescence decay kinetics with increasing partial pressures of oxygen. A new 'log-Gaussian distribution in τ_o or k_q' model is introduced which has the advantage over a Gaussian distribution model of placing no limitation on the value of ρ. However, a 'log-Gaussian distribution in τ_o' model generates Stern–Volmer quenching plots that show little degree in curvature, even at large ρ values and luminescence decays that become increasingly first order with increasing pO_2. In fact, with real optical oxygen sensors, the opposite is observed and thus the model appears of little value. In contrast, a 'log-Gaussian distribution in k_o' model does produce the trends observed with real optical oxygen sensors; although its use is restricted to

those in which the kinetics of luminescence decay are good first order in the absence of oxygen, such as the $[Ru(dpp)_3^{2+}(Ph_4B^-)_2]$ in cellulose optical oxygen sensor. It appears likely that a combination of a log-Gaussian distribution in k_o with one in τ_o will produce a model that is relevant to a much broader range of optical oxygen sensor, and this forms the basis of the next paper in this series.

Acknowledgement

The author thanks Ms. F. C. Williams for providing the data on the cellulose acetate based optical sensor.

References

1 A. Mills, *Platinum Met. Rev.*, 1997, **41**, 115.
2 M. L. Hitchman, *Measurement of Dissolved Oxygen*, John Wiley, Geneva, 1978, ch. 1.
3 O. S. Wolfbeis, in *Fibre Optic Chemical Sensors*, ed. O. S. Wolfbeis, Vol II, CRC Press, Boca Ranton, FL, 1991, ch. 10.
4 A. Mills, *Sens. Actuators B*, 1998, **51**, 69.
5 C. McDonagh, B. D. MacCraith and A. K. McEvoy, *Anal. Chem.*, 1998, **70**, 45.
6 E. R. Carraway, J. N. Demas and B. A. DeGraff, *Langmuir*, 1991, **7**, 2991.
7 J. R. Bacon and J. N. Demas, *Anal. Chem.*, 1987, **59**, 2780.
8 P. Hartmann and W. Trettnak, *Anal. Chem.*, 1996, **68**, 2615.
9 W. W-S. Lee, K-Y. Wong and X-M Li, *Anal. Chem.*, 1993, **65**, 255.
10 I. Klimat and O. S. Wolfbeis, *Anal. Chem.*, 1995, **67**, 3160.
11 H. N. McMurray, P. Douglas, C. Busa and M. S. Garley, *J. Photochem. Photobiol.*, 1994, **80**, 283.
12 E. R. Carraway, J. N. Demas, B. A. Degraff and J. R. Bacon, *Anal. Chem.*, 1991, **63**, 337.
13 L. Sacksteder, J. N. Demas and B. A. DeGraff, *Anal. Chem.*, 1993, **65**, 3480.
14 J. N. Demas, B. A. DeGraff and W. Xu, *Anal. Chem.*, 1995, **67**, 1377.
15 X-M Li and K-Y. Wong, *Anal. Chim. Acta*, 1992, **262**, 27.
16 X-M Li, F-C. Ruan and K-Y. Wong, *Analyst*, 1993, **118**, 289.
17 E. R. Carraway, J. N. Demas and B. A. DeGraff, *Anal. Chem.*, 1991, **63**, 332.
18 J. N. Demas and B. A. DeGraff, *SPIE*, 1992, **1681**, 2.
19 J. N. Demas and B. A. DeGraff, *Sens. Actuators*, 1993, **11**, 35.
20 S. Draxler, M. E. Lippitsch, I. Klimant, H. Kraus and O. S. Wolfbeis, *J. Phys. Chem.*, 1995, **99**, 3162.
21 M. L. Bossi, M. E. Daraio and P. F. Aramendia, *J. Photochem. Photobiol.*, 1999, **120**, 15.
22 P. M. Gewehr and D. T. Delpy, *Med. Biol. Eng. Comput.*, 1994, 659.
23 A. Mills and F. C. Williams, *Thin Solid Films*, 1997, **306**, 163.
24 P. Hartmann and W. Trettnak, *Anal. Chem.*, 1996, **68**, 2615.
25 W. Xu, R. C. McDonough, B. Langsdorf, J. N. Demas and B. A. DeGraff, *Anal. Chem.*, 1994, **66**, 4133.
26 P. Hartmann, M. J. P. Leiner and M. E. Lippitsch, *Anal. Chem.*, 1995, **67**, 88.
27 W. J. Albery, P. N. Bartlett, C. P. Wilde and J. R. Darwent, *J. Am. Chem. Soc.*, 1985, **107**, 1854.
28 G. T. Brown, J. R. Darwent and P. D. I. Fletcher, *J. Am. Chem. Soc.*, 1985, **107**, 6446.

Paper 9/02153A